Analyzing the hemispheric asymmetry in the thermospheric density response to geomagnetic storms

Ercha A,[1,2] Aaron J. Ridley,[1] Donghe Zhang,[2] and Zuo Xiao[2]

Received 12 October 2011; revised 23 May 2012; accepted 3 July 2012; published 17 August 2012.

[1] The thermospheric densities derived by CHAMP/STAR accelerometer within the time period from 01 May 2001 to 31 December 2007 are utilized to investigate the hemispheric asymmetry in response to strong storm driving conditions. The geomagnetic storms of 03–07 April 2004 are first studied since the storms occurred close to the vernal equinox, allowing the seasonal asymmetry to be eliminated to the greatest extent. The averaged density enhancements in the southern polar region were much larger than that in the northern polar region. The comparisons of density versus *Dst* and *Ap* index indicate a strong linear dependence with the slopes of the fitted lines in the southern hemisphere being 50% greater than that in the northern hemisphere. This effect can possibly be attributed to the non-symmetric geomagnetic field. 102 storm events are used to conduct a statistical analysis. For each storm, a linear fit is made between the averaged mass density and the *Dst* and *Ap* indices independently in each hemisphere. The seasonal variation of the intercepts and the slopes of the fitted lines are further explored. The baseline is strongly dependent on season, with the hemisphere receiving the larger amount of sunlight having larger density. The slopes showed considerable hemispheric differences around the vernal equinox yet no statistical differences around other seasons. It is speculated that competing mechanisms cancel each other during the solstices, while during the equinoxes, the lower magnetic field in the southern hemisphere may allow stronger ion flows, thereby causing more Joule heating. It is uncertain why the vernal equinox would be favored in this explanation though.

Citation: A, E., A. J. Ridley, D. Zhang, and Z. Xiao (2012), Analyzing the hemispheric asymmetry in the thermospheric density response to geomagnetic storms, *J. Geophys. Res.*, *117*, A08317, doi:10.1029/2011JA017259.

1. Introduction

[2] It has long been understood that the solar extreme ultraviolet (EUV) radiation, the auroral particle precipitation, and the high-latitude Joule heating are the predominant sources of energy input that greatly affect the dynamic processes of the tightly coupled thermosphere and ionosphere. Quantifying the hemispherically asymmetric responses of the thermospheric density and composition under the varying influence of EUV radiation and auroral precipitation have been an important subject of concern. Above all, the background energy deposition into the thermosphere due to the absorption of solar EUV radiation by photo-ionization and photo-dissociation is not time invariant. This mechanism has been discovered through the analysis of the ever-growing amount of satellite drag data. *Paetzold and Zschörner* [1961] found that the thermospheric density and composition exhibit a maximum near the equinoxes, a major minimum from May to August, and a secondary minimum near January. Many following studies have shown that the large-scale interhemispheric circulation induced by the asymmetric distribution of solar EUV heating can cause the seasonal variation of the background density of the thermosphere [e.g., *Johnson and Gottlieb*, 1970; *Mayr et al.*, 1978; *Fuller-Rowell*, 1998].

[3] In addition, dramatic enhancements of the Joule heating as well as large-scale perturbations in the thermospheric neutral density and composition caused by geomagnetic storms and substorms can be quite asymmetric [*Prölss*, 1987; *Forbes et al.*, 1996]. Significant amounts of momentum and energy are deposited into, the high-latitude regions of the upper atmosphere via Joule heating, which can be the dominant energy source into the global ionosphere and thermosphere [*Fuller-Rowell et al.*, 1994; *Meier et al.*, 2005; *Sutton et al.*, 2005]. The redistribution of energy and heat results in an increase of the scale height. Because of this, an enhancement of thermospheric neutral density would be expected at a constant altitude. For example, *Liu and Lühr* [2005], using the three-axes accelerometer on board the

[1]Department of Atmospheric, Oceanic and Space Sciences, University of Michigan, Ann Arbor, Michigan, USA.
[2]Institute of Space Physics and Applied Technology, Peking University, Beijing, China.

Corresponding author: A. J. Ridley, Department of Atmospheric, Oceanic and Space Sciences, University of Michigan, 2455 Hayward St., Ann Arbor, MI 48109, USA. (ridley@umich.edu)

0148-0227/12/2011JA017259

CHAMP satellite *Reigber et al.* [2002], showed that the storm-time enhancement of the thermospheric density at approximately 400 km reached 400% of quiet time values during the geomagnetic storms occurring on 29–30 October, 2003. *Liu et al.* [2005] utilized one year of data from the CHAMP satellite to show that the thermospheric density enhancement is highly structured at high latitudes. A high-resolution model of the global thermosphere used by *Demars and Schunk* [2007], showed that the density enhancements observed by the CHAMP satellite could result from sufficiently strong heating in the cusp. Some studies show that small-scale field-aligned current filaments observed in the cusp region can play an important role in heating the thermosphere, thus leading to significant density enhancements [e.g., *Griffis et al.*, 1981; *Neubert and Christiansen*, 2003; *Lühr et al.*, 2004]. Moreover, the intensified Joule and particle heating in the auroral oval can cause strong upwelling of the atmosphere, which transports nitrogen-rich or oxygen-depleted air upward in the thermosphere [*Prölss*, 1980], and can drive an increased pressure-gradient force, which leads to enhanced meridional winds *Burns et al.* [1995]. The deviation from the diffusive equilibrium as well as the barometric motion lead to variations of O/N_2 ratio at a constant height [*Rishbeth et al.*, 1987].

[4] Some studies have indicated that there are hemispheric asymmetries in thermospheric density response to external driving. For example, the geomagnetic storm that happened on 20–21 November 2003 was investigated by *Bruinsma et al.* [2006] using data from the CHAMP and GRACE satellites. Results revealed that both the dayside and nightside density response at north 72° magnetic latitude were smaller compared to those at the magnetically conjugate latitude. This asymmetric phenomenon was explained by enhanced conductances in the southern hemisphere that facilitate the flow of currents and thereby the Joule heating.

[5] However, it is still unclear whether there are strong asymmetries in electric fields, auroral precipitation, and Joule heating. First, when either pole tilts more toward the Sun, the seasonal variation of the solar UV illumination may generate asymmetries in ionospheric conductivity. The changes in conductivities will further alter the profile of plasma convection [*Ridley et al.*, 2004; *Ridley*, 2007] and influence the field-aligned currents [*Christiansen et al.*, 2002; *Wang et al.*, 2005]. Thus one might expect a hemispherically asymmetric electric potential pattern, which has been explored by some studies recently using SuperDARN radar [e.g., *Shepherd et al.*, 2002, 2003; *Lukianova et al.*, 2008; *Lukianova and Christiansen*, 2008; *Koustov et al.*, 2009; *Pettigrew et al.*, 2010]. Second, there are also asymmetries in the auroral particle precipitation. *Newell et al.* [1996] proposed that the occurrence of the accelerated electron beams lead to discrete aurora that are much stronger in darkness than in sunlit conditions, which means the winter and nightside hemispheres get more aurora than the summer and dayside hemispheres. *Collin et al.* [1998] also found that in winter, most of the upward flowing ion beams occurred between 1500∼0100 MLT with a peak existing 2 hours before midnight, while the occurrence rate is low with no clear peak in the summer. This dark-favored phenomenon for auroral precipitation has been investigated by many studies [e.g., *Erlandson and Zanetti*, 1998; *Kumamoto and Oya*, 1998]. Third, the Earth's magnetic field is non-symmetric, with a larger tilt angle and increased offset in the southern hemisphere. This phenomenon may facilitate the electrodynamic coupling between the geomagnetic field and the solar wind, thus further strengthening the plasma drifts in the southern hemisphere [*Bruinsma et al.*, 2006]. It is unknown whether the asymmetries in the aurora (and therefore the ionospheric conductances) between the winter and summer hemispheres, coupled with the asymmetries in the field-aligned currents produce an asymmetric pattern in the ionospheric potential. Further, because of the differences in the magnetic field, it is also not clear if the ion drifts or Joule heating should be symmetric or not.

[6] An important goal, therefore, is to specify how and to what degree the thermospheric asymmetric density and composition response can be attributed to asymmetric electrodynamic drivers. Isolated storm events have been widely studied by many researchers via incoherent scatter radar, global satellites, and models [e.g., *Huang et al.*, 2005; *Liu and Lühr*, 2005]. However, few studies focused on providing a reasonable explanation of hemispheric asymmetry in the density response. Moreover, little work has been done to investigate the long-term trends of hemispheric asymmetry under strong storm driving conditions.

[7] In the present paper, we first analyze a specific storm event measured by the CHAllenging Minisatellite Payload (CHAMP) near vernal equinox to illustrate an example of hemispheric asymmetry in the density responses. Then a combined data set of 102 storm-interval events during 2001–2007 are presented. We attempt to focus on the following two perspectives: (1) exploring the hemispheric asymmetry in the high latitude density perturbation in terms of the electrodynamic drivers and geomagnetic field; and (2) examining the seasonal variation of hemispherical asymmetry in the density response.

2. Brief Description of CHAMP Satellite

[8] CHAMP was launched into an approximately circular polar-orbit with an inclination of 87.3° and an altitude around 454 km on 15 July 2000. The mission was designed with the primary plan to explore the magnetic field and the gravity of the Earth, and with a secondary perspective of investigating the upper atmosphere [*Reigber et al.*, 2002]. The polar orbit ensured that CHAMP could provide global-scale coverage with traces mainly concentrated in two local time sectors for most latitudes. Figure 1 shows CHAMP satellite orbits as a function of local time and latitude on 03–07 April 2004 to depict this feature. CHAMP had complementary payload elements (magnetometer, accelerometer, star sensor, GPS receiver, laser retro reflector, ion drift meter), which made it possible to simultaneously measure ionospheric and thermospheric parameters such as neutral density, electron density, temperature, and magnetic field. One of the most relevant instruments on board was the Spatial Triaxial Accelerometer for Research (STAR) with 0.1 Hz sampling rate and with a resolution of 3×10^{-9} ms^{-2} in y-axis and z-axis and 3×10^{-8} ms^{-2} in x-axis. The high spatial and temporal resolution of STAR made it capable of measuring the thermospheric mass density with resolution as fine as 10^{-14} kg m^{-3}, which affords an excellent opportunity to study the asymmetric thermospheric density response to severe storm driving conditions. For further details on the

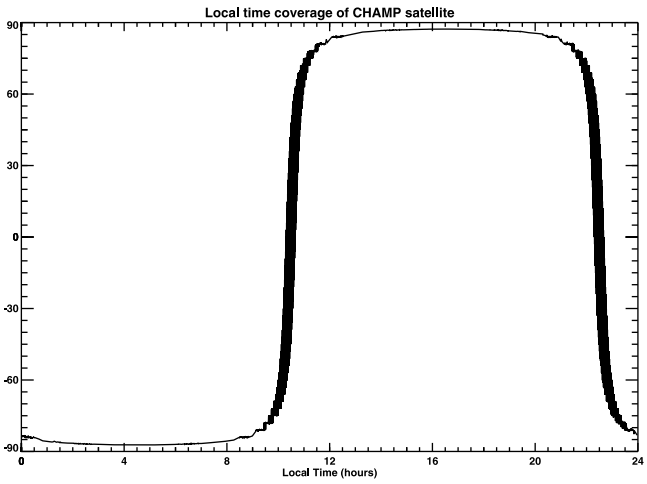

Figure 1. Latitude versus local time for CHAMP satellite orbit during 03–07 April 2004.

procedure of density derivation and error estimation, readers may refer to *Liu et al.* [2005], *Bruinsma et al.* [2004], and *Sutton et al.* [2005].

[9] The thermospheric density derived from the CHAMP/STAR accelerometer was smoothed over 10 s, which corresponds to around 80 km resolution along the satellite track. Spurious spikes were removed also. The orbit altitude of the CHAMP satellite decayed from an initial 454 km in the year of 2000 to 330 km in the year of 2007. The hemispheric altitude differences were as much as 30 km due to the slightly elliptical orbit. Usually, the neutral densities were normalized to a certain height to exclude the systematic difference induced by the variation of orbit height [e.g., *Prölss*, 1980; *Liu et al.*, 2005]. However, the normalization during disturbed times, when the thermosphere severely departs from diffusive equilibrium, can add relatively large errors. Therefore, the normalization is not implemented in the current study, while the relative difference of thermospheric density was used to avoid the influence due to altitude dependence of density response as much as possible.

3. The 03–07 April 2004 Geomagnetic Storm Event

3.1. Solar Wind IMF and Geomagnetic Activity Indices

[10] The magnetic storm of 03–07 April 2004 was selected for the present study, as there were two continuous large geomagnetic disturbances in a relatively short time, which occurred quite close to the vernal equinox. This storm event provided an excellent opportunity to investigate the hemispherically asymmetric density response. Figure 2 displays the solar wind and IMF data adjusted to 1 AU from Advanced Composition Explorer (ACE) spacecraft as well as the *Ap* and *Dst* indices during 03–07 April 2004. Two continuous storm sudden commencements (SSCs) that occurred at 0946 UT and 1410 UT on 03 April 2004 are also marked in the panels. The sign of IMF B_z changed rapidly during this interval. It shifted northward immediately after the first SSC and reached 10 nT at around 1130 UT, then decreased abruptly followed by a second increase close to the SSC that occurred around 1410 UT and stayed southward for 10 hours before turning northward again. One important phenomenon worth noting is a sign change of IMF B_x and B_y at 0030 UT on 04 April 2004 just before the *Dst* index reached a minimum value of −115 nT. This characteristic is also reflected with a second increase in the *Ap* index around the same time. Similar conditions with sharp sign changes in IMF also occurred in the following geomagnetic disturbances at around 1930 UT on 05 April 2004.

3.2. Asymmetries in High Latitudes Density Responses

[11] Figure 3 (top) displays the thermospheric neutral density derived by the CHAMP/STAR accelerometer along satellite track in daytime (top left) and nighttime (top right) respectively. The variation of *Ap* and *Dst* index are also shown in Figure 3. The density responses are plotted as a function of the universal time (UT) and geographic latitude. The CHAMP dayside local times are confined in the range of 1020–1040 LT, while the nighttime local times are confined in the range of 2220–2240 LT. For the daytime density responses (top left), the first remarkable density enhancements can be seen around 1000 UT, right after the first SSC, in the northern hemispheric latitude range of 50° to 80°. The same kind of density enhancements can also be observed in the southern hemisphere starting from 1430 UT. The 4 hour time difference between the response of two hemispheres might be attributed to the phenomenon that the CHAMP satellite did not pass through a region in the high latitudes that has been affected yet. This could happen if the disturbance happened in a

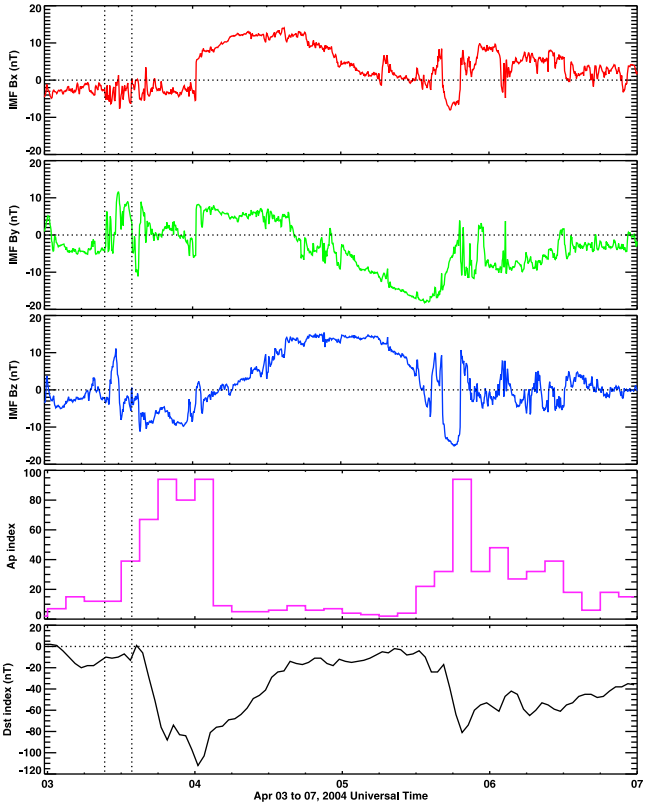

Figure 2. Variation of the IMF, *Ap*, and *Dst* index during 03–07 April 2004 storm events. The storm sudden commencements (SSCs) occurred at 0946 UT and 1410 UT on 03 April 2004.

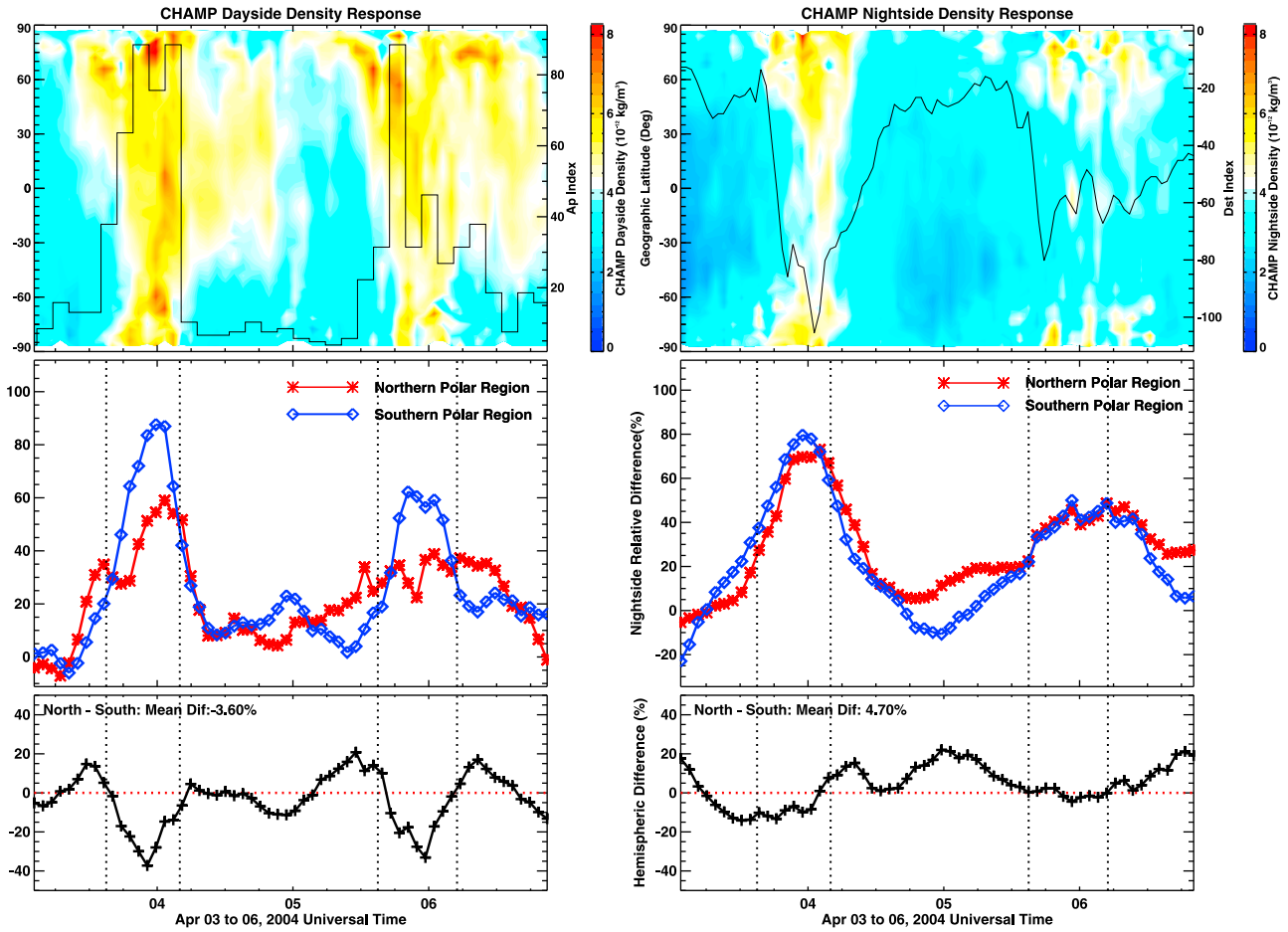

Figure 3. Thermospheric neutral density along satellite track with latitude versus universal time in (top left) dayside and (top right) nightside. The *Dst* and *Ap* index are also shown in the top left and top right, respectively. Relative deviation of thermospheric density at northern polar region (60°–90°N) and southern polar region (60°–90°S) in (middle left) dayside and (middle right) nightside. Hemispheric difference in (bottom left) dayside and in (bottom right) nightside. The sector between the 1st and 2nd (3rd and 4th) vertical dotted lines represented the time period among strong driving conditions with *Ap* index ≥ 30.

different local time sector. A. J. Ridley (Universal time effect in the response of the thermosphere to electric field changes, manuscript in preparation, 2012) found that there are universal time dependence in the thermospheric response to external driving between the northern and southern hemispheres. In the northern hemisphere, the thermospheric density has larger response when the perturbation occurs early in the day, but a more subdued response when the perturbation occurs later in the day. For the southern hemisphere, the trends are roughly opposite. This is coincident with the phenomenon that the northern hemisphere reacted with more efficiency to the first SSC at 0946 UT and the southern hemisphere reacted with more efficiency to the second SSC at 1410 UT. Note from the IMF B_z in Figure 2, the strong disturbance of the thermospheric density occurred right after B_z turned southward. The pronounced density enhancements then occurred in a wide range across the polar region both in the northern and southern hemispheres. The density disturbances subsequently propagated towards the middle and low latitude regions with somewhat weaker responses being measured. And finally, the density enhancements appeared in the equatorial region with a 6-hour time delay after the large-scale density response occurred in the polar region. The corresponding wave speed was about 500 m/s. A second large-scale density enhancement in the polar regions occurred around 1600 UT on 05 April 2004, after the IMF B_z shifted southward suddenly, reaching a minimum value of −16 nT. On the nightside (Figure 3, top right), the maximum value of the thermospheric density response was less than that of the dayside, but the basic characteristics of the density disturbances in the polar regions and the propagation towards the equatorial region were similar as on the dayside.

[12] Discrepancies in the density response do exist between different areas; especially between day and night. In addition, the altitude dependence of absolute density response adds systematic errors due to the variation of orbit height in two hemispheres. Therefore, a much better perspective on describing the hemispheric response to external driving is to examine the relative density deviation from values of geomagnetic quiet time (i.e., $(\rho_{disturbed} - \rho_{quiet})/\rho_{quiet}$). The densities measured just prior to the storm are used as the quiet time densities. Figure 3 (middle) shows the relative difference of the neutral density compared to the density on April 2nd averaged across the northern polar region

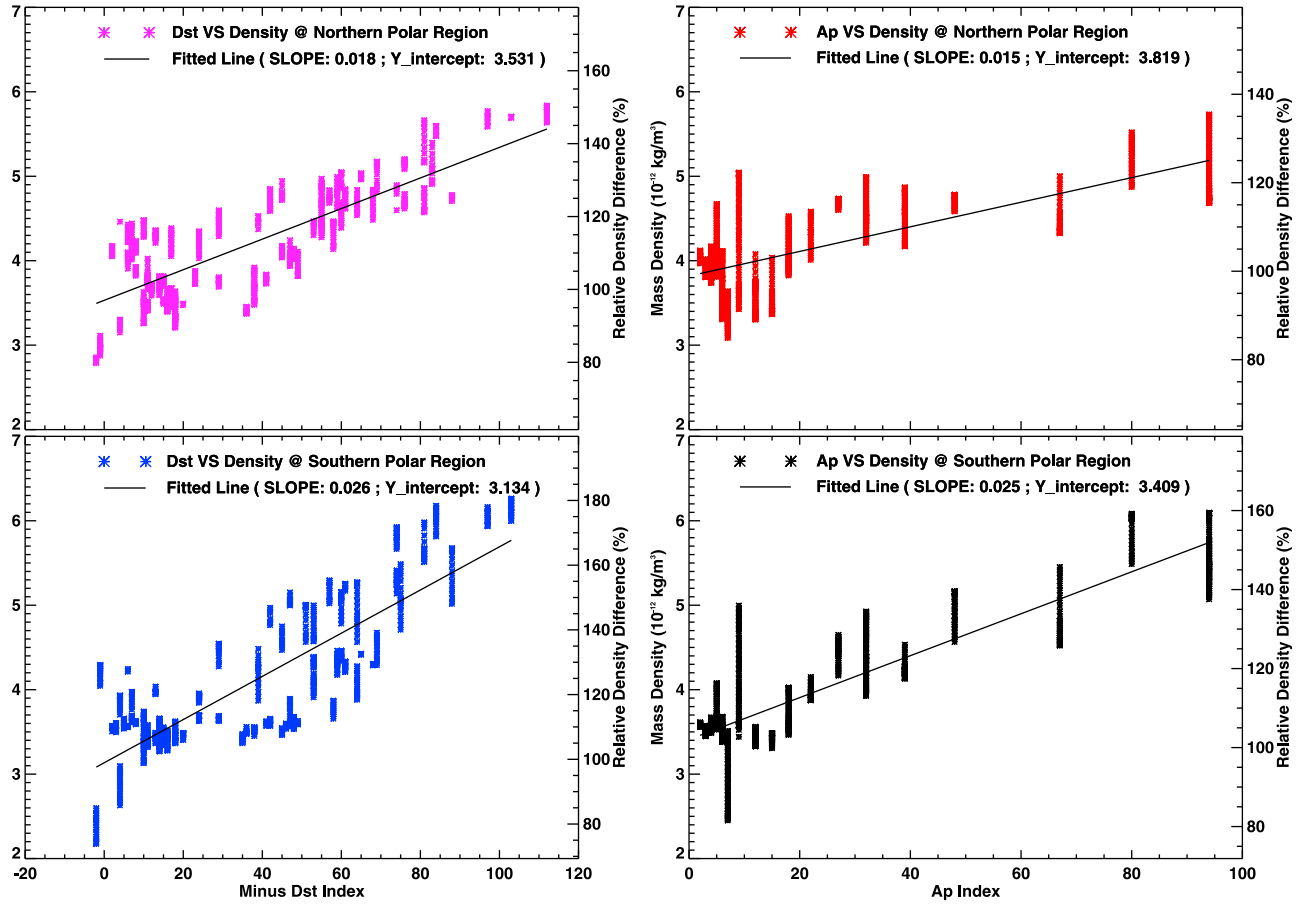

Figure 4. The thermospheric density versus minus *Dst* index for (top left) northern hemisphere and (bottom left) southern hemisphere. The thermospheric density versus *Ap* index for (top right) northern hemisphere (bottom right) and southern hemisphere. The relative density difference is represented via the right Y-axis.

(60°–90°N) and southern polar region (60°–90°S) for the daytime (middle left) and nighttime (middle right) parts of the orbit respectively. Significant density enhancements occurred accompanying the considerable elevation of the *Ap* index and decreasing of the *Dst* index. However, it can be seen that the storm-time relative differences averaged across the polar region are non-symmetric between the northern and southern hemispheres. For the daytime density disturbances during the main phase of the storm on 04 April 2004, the maximum density enhancement in southern polar region, about 90%, is evidently larger than that in northern polar region, which increased by 60%. The 2nd peak of relative density response, corresponds to the storm that occurred on 05 April, is also larger in the southern polar region, about twice the value of density enhancement in the northern hemisphere. Moreover, hemispheric asymmetries also existed in the nighttime density responses, although with significantly smaller differences between the northern and southern hemispheres.

[13] The bottom panels display the hemispheric differences of density enhancements in the polar region. The sectors between the 1st and 2nd as well as the 3rd and 4th vertical dotted lines in the middle and bottom panels represent the strong storm driving conditions with *Ap* index $\geq$ 30. The southern hemisphere reacts stronger under high polar driving conditions for the daytime and somewhat for the nighttime conditions.

[14] In order to determine quantitatively the asymmetric response of the thermospheric density to the two storms, the *Dst* index and the *Ap* index were compared to the averaged CHAMP neutral densities in the northern polar region (60°N–90°N) and southern polar region (60°S–90°S). The results are shown in Figure 4 with scatterplots of densities as a function of minus *Dst* index (left panels) and of *Ap* index (right panels). There is a clear linear dependence in each of the four panels, indicated by the least squares fitted lines. This phenomenon, which is coincident with what we have described in Figure 3 and in section 1, can be attributed to the increased scale height due to Joule heating in polar region. The slope and the intercept of the fitted lines are also calculated and marked in Figure 4. The slopes are 0.530 and 0.409 in northern hemisphere for the *Dst* and *Ap* indices respectively, while the corresponding slopes are 0.818 and 0.699 in southern hemisphere. Therefore, the slopes in the southern hemisphere are about 50% greater than those in the northern hemisphere. As for the base values of thermospheric density under unperturbed conditions (i.e., the y-intercepts), the value of northern hemisphere is a little bit larger than that in southern hemisphere, which is due to the

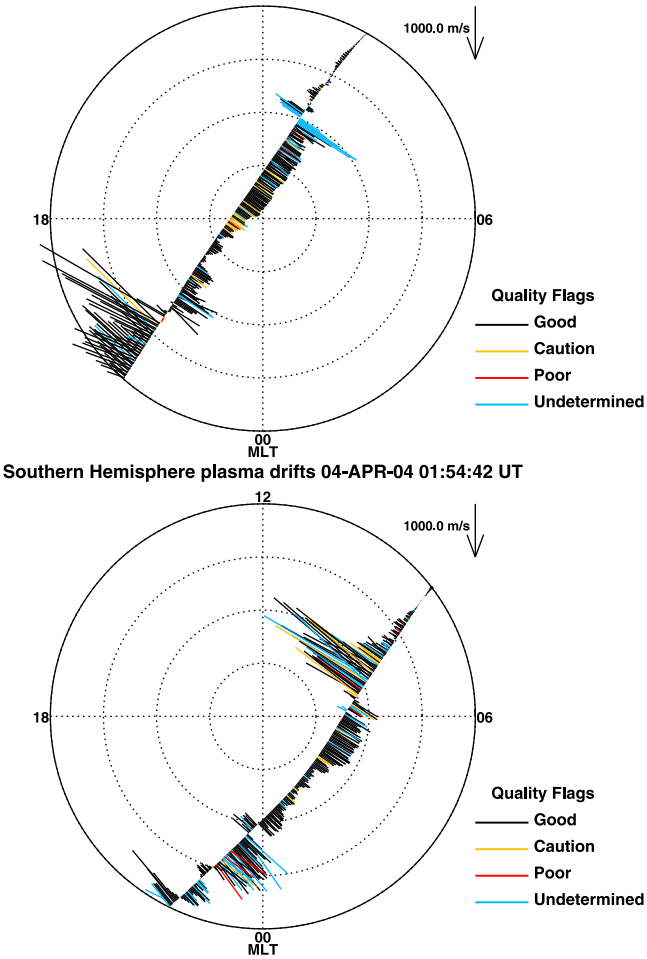

Figure 5. Cross-track plasma drift of DMSP F15 on April 4, 2004. The outer ring corresponds to 50° (−50°) magnetic latitude for northern (southern) hemisphere.

northern hemisphere being slightly warmer just after the vernal equinox.

[15] The hemispheric asymmetry in the slopes may be attributed to several factors including the asymmetric electrical conductivity, asymmetric plasma convection flow and non-symmetric geomagnetic field. As the storm event is close to the vernal equinox, the polar regions of the two hemispheres are subject to the similar solar zenith angle (although the northern hemisphere has a slightly smaller solar zenith angle). This will not bring about significant hemispheric differences in the electrical conductivity. As for the plasma convection flow, Figure 5 shows the cross-track plasma drifts measured by Defense Meteorological Satellite Program (DMSP) F15 spacecraft (0928–2128 LT orbit) at around 0106 UT for northern polar region and around 0154 UT for southern polar region on April 4, 2004. The plasma drift in the southern hemisphere is stronger than the drift in the northern hemisphere on the dayside, which is an indication that the Joule, or frictional, heating may be stronger in the southern hemisphere. On the dayside between the 50°–60° latitude, the northern hemisphere has larger ion pattern. *Bruinsma et al.* [2006] pointed out that the stronger plasma drifts in southern hemisphere may be related to Earth's asymmetric magnetic field with a relatively larger tilt angle in the southern hemisphere and a northward offset in the location of the dipole. This asymmetry can boost the interaction between the solar wind flow and the geomagnetic field in the southern hemisphere compared to the northern hemisphere, and hence advance the electrodynamic coupling. Complicating matters the abrupt change of IMF B_y at 0030 UT, most likely caused the high-latitude ion convection systems to change significantly. For the positive IMF B_y, the convection cell in dusk region of northern hemisphere increases in size relative to its counterpart *Weimer* [1996]. Therefore, In order to better determine whether this phenomenon is similar for different disturbed conditions, a statistical study is conducted examining a large number of storm periods.

4. The Seasonal Variation of Hemispheric Asymmetry Observed by CHAMP

[16] Figure 6 shows the orbit-averaged CHAMP thermospheric densities in the northern polar region (60°N–90°N), southern polar region (60°S–90°S), and global scale average during the time period from 01 May 2001 to 31 December 2007. The variation of the *Dst* index and *Ap* index are shown. Further, the percentage difference in mass density between the northern and southern hemispheres is also shown. The most conspicuous features on the general level of density are the decaying solar cycle and the seasonal

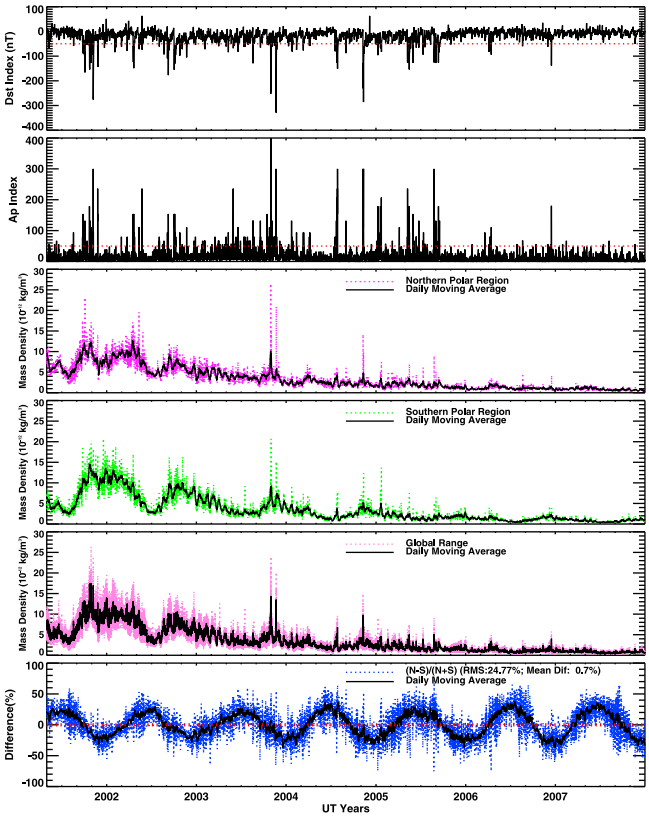

Figure 6. Long-term variation of the *Dst* index, *Ap* index, neutral density in northern polar region, neutral density in southern polar region, global averaged neutral density, and the hemispheric relative difference during May 1, 2001–Dec 31, 2007.

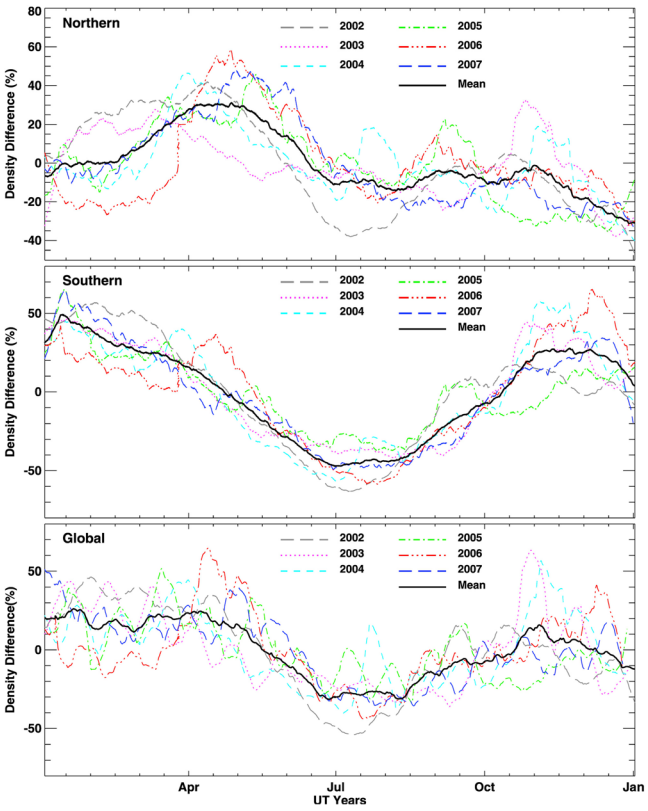

Figure 7. Thermospheric density difference over the course of the year for (top) northern hemisphere, (middle) southern hemisphere, and (bottom) global average during 2002–2007.

variation. In addition, there appears to be a direct relationship between the thermospheric density and geomagnetic activity in both hemispheres. This phenomenon is consistent with what we analyzed for the storm event on 03–07 April 2004. The percent difference between the two hemispheres and the root mean square difference (RMS) are calculated and shown in Figure 6 (bottom). The warmer summer hemisphere dominates since the cyclical fluctuation of percent difference exhibits an annual periodicity with maxima near the June solstice and minima around the December solstice. Another thing worth noting is that there are solar cycle, annual, seasonal, and solar rotational variation components in the density for both hemispheres.

[17] Figure 7 shows the variation of mass density difference ($\rho_{Difference}$) over the course of the year as follows:

$$\rho_{Difference} = \frac{\rho - \overline{\rho_{year}}}{\overline{\rho_{year}}} \times 100\%, \quad (1)$$

where $\overline{\rho_{year}}$ is the hemispherical mass density averaged over a year. We can see that the variation of density difference in the northern and southern hemispheres are radically different from each other. Normally one would expect peaks at summer solstice and minimum at winter solstice, which is consistent with the situation represented in the southern hemisphere. However, the northern hemisphere has some different characteristics with a major peak around April and a significantly smaller peak in late autumn. The expectation is that, in the summer, the density should maximize and in the winter, the density should minimize. The southern hemisphere clearly shows this behavior, while the northern hemisphere does not. It is unclear why the northern and southern hemisphere differ in their annual behavior. The global-scale feature of the density difference is a combination of the northern and southern hemispheres, which exhibits a maximum near the equinoxes, a major minimum around June solstice, and a secondary minimum near the December solstice. This phenomenon is roughly consistent with pre-existing theory of seasonal asymmetry in thermospheric density [*Paetzold and Zschörner*, 1961], which is considered to be caused by less diffusive separation of the species at solstice, resulting from the global-scale, interhemispheric circulation [*Johnson and Gottlieb*, 1970; *Mayr et al.*, 1978; *Fuller-Rowell*, 1998].Another thing worth noting is that the variation between seasons in the southern hemisphere is much larger than that in the northern hemisphere, which might illustrate that the southern hemisphere is more susceptible to external solar EUV driving.

[18] To further investigate the hemispheric asymmetry, 102 major storm events between 01 May 2001 and 31 December 2007 were selected for study of the seasonal variation of the asymmetric response of the system to energy input. An event is only considered if the conditions *Dst* index < -50 and *Ap* index > 50 appeared simultaneously. Table 1 shows a break down of the events by year and season.

[19] For each single storm event, the thermospheric neutral densities for the two hemispheres were compared with the *Dst* and *Ap* indices, and the slopes and intercepts were calculated as described in section 3. Figure 8 shows the seasonally classified collection of the slopes for neutral density versus *Dst* indices both in the northern and southern hemispheres. The median slope of each seasonal group is calculated and indicated on the plots. Figure 9 displays the seasonally classified probabilities distribution of the slopes for neutral density versus *Dst* and *Ap* indices in two hemispheres. Of particular attention is whether the slopes and intercepts of two hemispheres are statistically different from each other in the four seasons. If there are differences, then further exploration needs to be implemented to determine which hemisphere dominates. The above question is assessed using the Student's T-test with the t-statistic calculated by the following formula:

$$t = \frac{\overline{X_N} - \overline{X_S}}{\sqrt{\frac{VAR_N}{n_N} + \frac{VAR_S}{n_S}}}, \quad (2)$$

Table 1. Seasonal Division of 102 Storm Events

	Spring (Mar, Apr, May)	Summer (Jun, Jul, Aug)	Autumn (Sep, Oct, Nov)	Winter (Dec, Jan, Feb)	Total
2001	0	5	7	2	14
2002	5	2	8	5	20
2003	6	8	5	3	22
2004	2	3	3	4	12
2005	6	5	3	5	19
2006	4	2	3	1	10
2007	3	0	2	0	5
Total	26	25	31	20	102

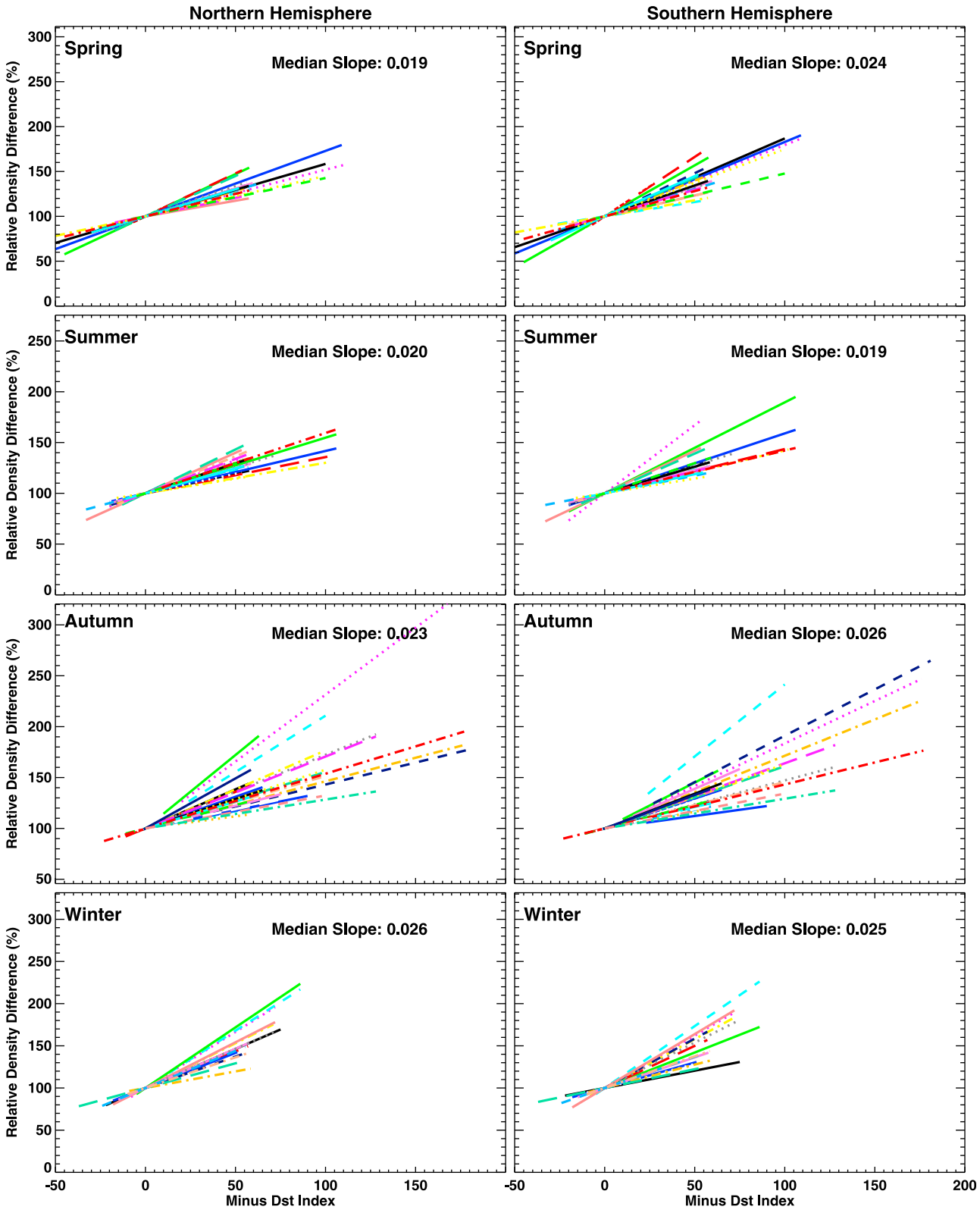

Figure 8. Minus *Dst* index versus relative density difference via linear regression analysis (left) in the northern hemisphere and (right) in the southern hemisphere. The y-intercept of each line has been removed and set to 100%.

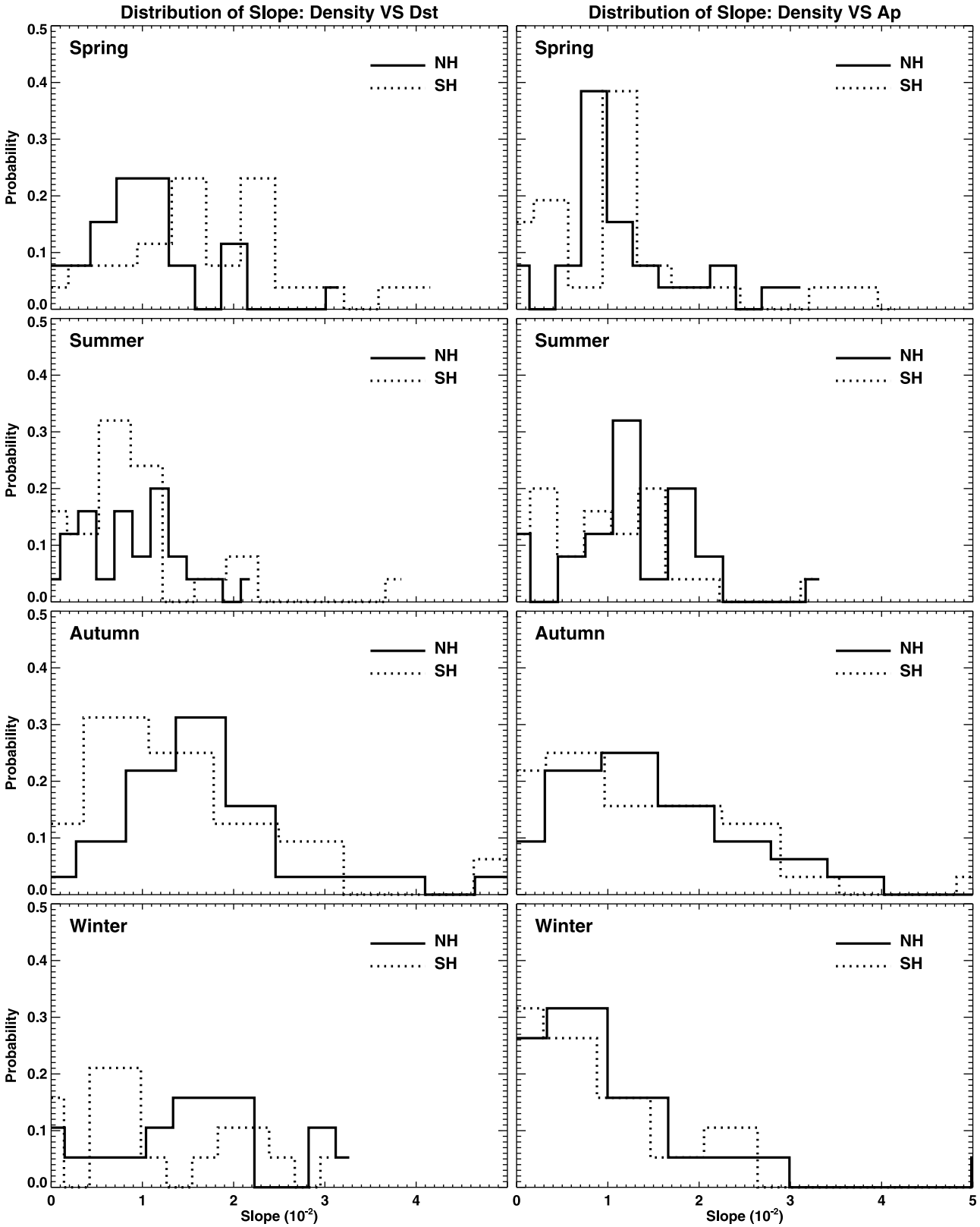

Figure 9. The probability distribution of slopes in two hemispheres for (left) density versus *Dst* and (right) density versus *Ap*.

Table 2. T-Test of 102 Storm Events[a]

Season (North)	T Value: Slope (Density Versus *Dst*)	T Value: Slope (Density Versus *Ap*)	T Value: Intercept (Density Versus *Dst*)	T Value: Intercept (Density Versus *Ap*)	Degrees of Freedom	t_{95}
Spring	**−1.784**	**−1.803**	0.713	0.739	50	1.676
Summer	−0.075	−0.260	**2.629**	**2.763**	48	1.684
Autumn	−0.125	−0.343	−1.155	−1.025	60	1.671
Winter	0.326	0.019	**−1.754**	**−1.815**	38	1.697

[a]The bold numbers represent a rejection of the null hypothesis.

where $\overline{X_N}$ and $\overline{X_S}$ are the mean values of the slopes or intercepts in the northern and southern hemisphere respectively, while *VAR* is the variance and *n* is the sample size. The calculated T-value with associated degrees of freedom is then compared to the critical T-value from the distribution table with the specified confidence level (usually 95%). The results are listed in Table 2. The bold numbers represent a rejection of the null hypothesis, i.e., bold means that the two hemispheres are statistically different from each other. It can be seen from the T-values of the slopes that the two hemispheres react asymmetrically in northern Spring with the southern hemisphere more susceptible to the storm driving due to the minus sign of T-value. This phenomenon is consistent with what was found for the storm event on 03–07 April 2004. For the slopes, no other season showed a significant hemispheric asymmetry. As for the intercepts, the summer hemisphere is always favored due to more EUV radiation. This is consistent with the analysis in Figures 6 and 7.

[20] Another perspective on the linear dependence of the neutral density on the *Dst* and *Ap* indices is provided in Figure 10. The slope of the fitted line for density versus *Dst* and density versus *Ap* for each storm event are represented in the form of seasonal variation in the top panels. The fluctuations of the intercept for the fitted lines are shown in the bottom panels. Pronounced hemispheric asymmetries are seen in the seasonal variation of the intercept lines, while there exists some time periods in which there is a hemispheric asymmetry in the slopes. The values of the slopes for density versus *Dst* in the southern hemisphere are larger than those in the northern hemisphere (Figure 10a) during two periods. One is roughly from March to May (around vernal

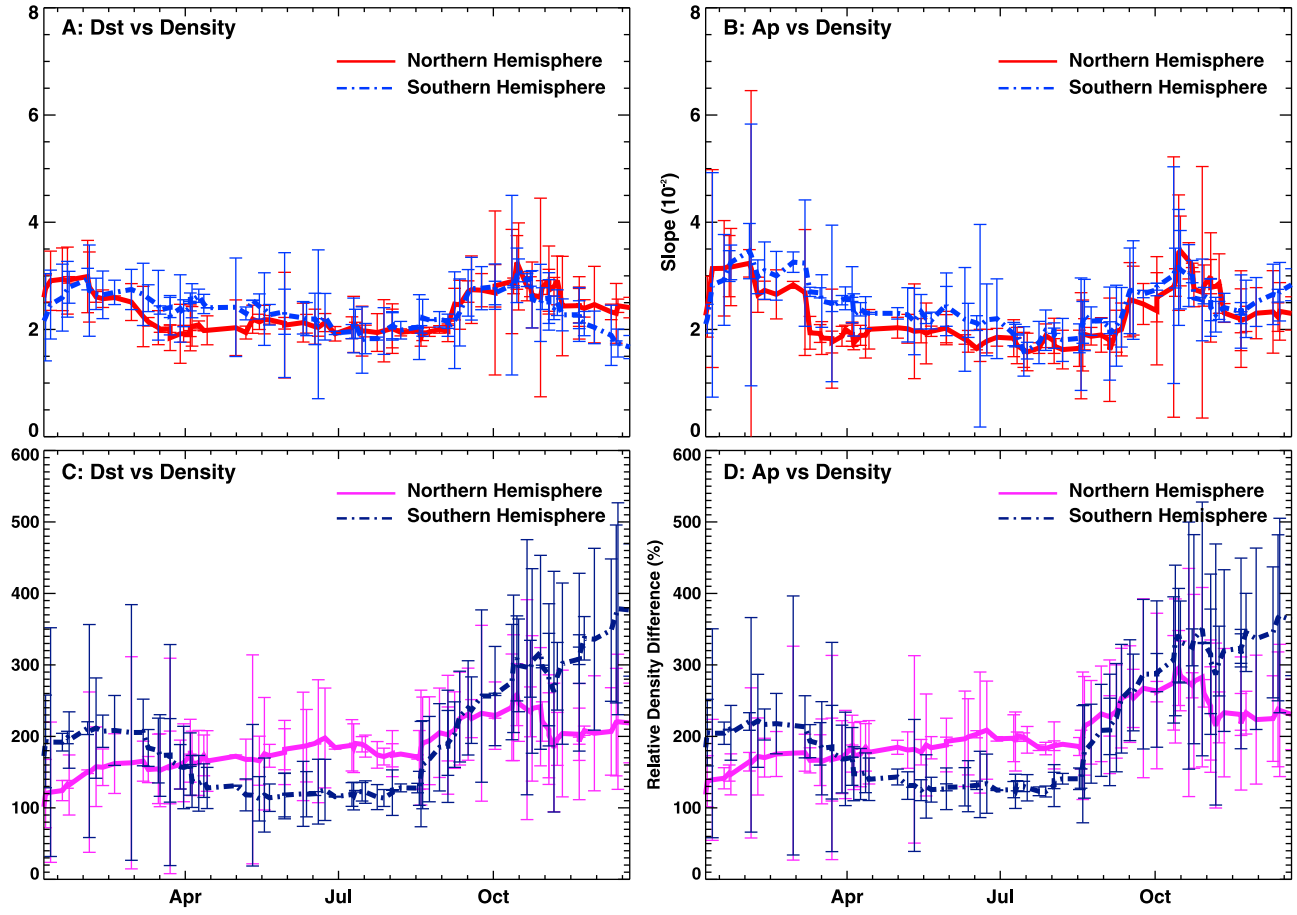

Figure 10. Seasonal variation of the slope of fitted line for (a) *Dst* versus density and (b) *Ap* versus density. Seasonal variation of the relative density difference of fitted line for (c) *Dst* versus density and (d) *Ap* versus density. Error bars are overlapping on each panel.

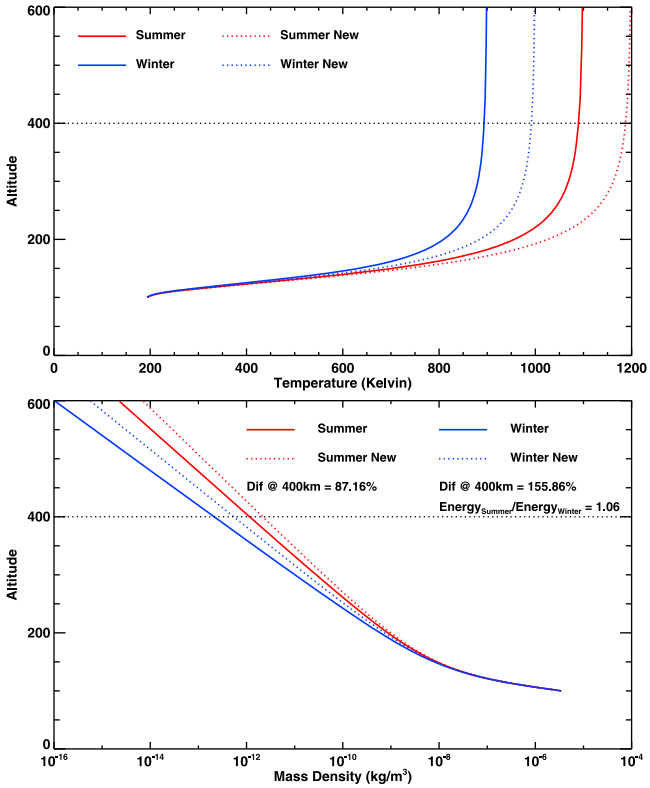

Figure 11. (top) The thermospheric temperature variation versus altitude in summer and winter before and after a temperature increase of 100 K calculated by J77. (bottom) The corresponding distribution of mass density versus altitude and the density difference at 400 km for summer and winter.

equinox), while the other is roughly from September to November (around autumnal equinox). The differences around both solstices between the two hemispheres are relatively small though, with the values around vernal equinox considered statistically different. The characteristics of slope lines for density versus *Ap* index (Figure 10b) are almost the same as those of the density versus *Dst* index. The values of the intercept lines in the summer hemisphere are larger than that of the winter hemisphere with the cross over occurring at the vernal and autumnal equinoxes as one would expect, since it reflects the characteristic of thermospheric density with seasonal variation of EUV illumination. It is interesting to note that the intercept trends for the southern hemisphere are very similar to the density variations throughout the year (Figure 7, middle), with a peak during the summer and minimum in the winter. In the northern hemisphere, the trend of being roughly constant through the year is the same, but the density variation (Figure 7, top) shows a peak near spring, while the intercepts show a peak near autumn.

5. Discussion

[21] The above results indicate that considerable hemispheric differences can be found around vernal equinox with the southern hemisphere reacting stronger, but no statistical differences can be found during other seasons.

[22] A possible explanation for this is that during summer and winter different effects may cancel each other out. The thermosphere model of *Jacchia* [1977] is used to further discuss this phenomenon. The J77 model calculate the thermospheric density and the temperature for given exospheric temperature T_∞. It was assumed by J77 that the upper atmosphere being composed of N_2, O_2, O, He, and H with all species sharing the same temperature profiles. Those species are considered well mixed below 90 km. A constant value T_0 = 188 K at the height Z_0 = 90 km is assigned. Above 90 km, all species are in diffusive equilibrium specified by temperature profiles, which rise to an inflection point at Z_x = 125 km, and become asymptotic to exospheric temperature T_∞. The temperature T_x and the temperature gradient G_x at the inflection point is defined as follows:

$$T_x = T_0 + 110.5\,\sinh^{-1}[0.0045(T_\infty - T_0)], \tag{3}$$

$$G_x = 1.9\left(\frac{T_x - T_0}{z_x - z_0}\right), \tag{4}$$

For $90 \le z \le 125$ km, The temperature profiles are given by the following:

$$T(z) = T_x + \frac{T_x - T_0}{\pi/2}\tan^{-1} \cdot \left\{\frac{G_x}{(T_x - T_0)/(\pi/2)}(z - z_x)\left[1 + 1.7\left(\frac{z - z_x}{z - z_0}\right)^2\right]\right\}, \tag{5}$$

For $z \ge 125$ km, The temperature profiles are given by the following:

$$T(z) = T_x + \frac{T_\infty - T_x}{\pi/2}\tan^{-1} \cdot \left\{\frac{G_x}{(T_\infty - T_x)/(\pi/2)}(z - z_x)\left[1 + 5.5 \times 10^{-5}(z - z_x)^2\right]\right\}. \tag{6}$$

Readers may refer to *Jacchia* [1977] for more details about the J77 model.

[23] Figure 11 (top) illustrates the temperature profiles of thermosphere calculated by J77 for summer and winter respectively. The bottom panel displays the corresponding distribution of mass density versus altitude. A exospheric temperature increase of 100 K is then added in each hemisphere and the relative change in the mass density at 400 km altitude is calculated and displayed. Since CHAMP measures the mass density, which has an integral effect given a temperature change, the relative difference of mass density for the same temperature change in a cold hemisphere is larger than that for a warm hemisphere, which was confirmed by Figure 11. This means that for a given temperature change, the winter hemisphere should have a larger relative change in mass density than the summer hemisphere.

[24] In addition, the local temperature change is proportional to the amount of thermospheric energy put into the system. The total thermospheric energy density can be described as the sum of the thermal $\eta_T(r) = C_V(r)n(r)T(r)/A$ [*Burke et al.*, 2009], and the gravitational potential energy $\phi_G(r) = \rho(r)M_E G/r$ *Wilson et al.* [2006]. Where $r = R_E + h$ is the distance from Earth's center; $C_V(r)$ is the heat capacity; $n(r)$ is the number density; $T(r)$ is the thermospheric temperature; A is the Avogadro's number; $\rho(r)$ is the mass density; M_E and G represent

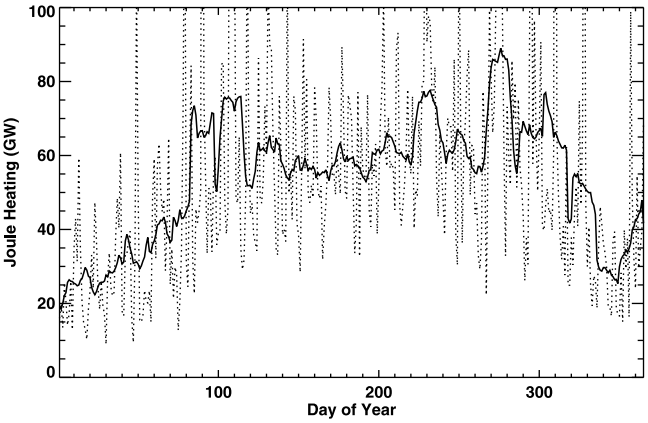

Figure 12. The daily Joule heating in northern hemisphere averaged over 3 years: 1999, 2000, and 2001.

the Earth's mass and the gravitational constant, respectively. In order to estimate the total energy of thermosphere $E_{th} = H_T + \Phi_G$, the thermal energy H_T and the gravitational energy Φ_G could be calculated as follows:

$$H_T \approx 4\pi \int_{R_E+h_0}^{R_E+1000} \eta(r) r^2 dr = \frac{4\pi}{A} \int_{R_E+h_0}^{R_E+1000} C_V(r) n(r) T(r) r^2 dr, \tag{7}$$

$$\Phi_G \approx 4\pi \int_{R_E+h_0}^{R_E+1000} [\phi(r) - \phi(r_0)] r^2 dr = 4\pi M_E G \int_{R_E+h_0}^{R_E+1000} \rho(r) \left[\frac{1}{r} - \frac{1}{r_0}\right] r^2 dr. \tag{8}$$

For more details on the mathematical descriptions of the thermospheric energy, readers may refer to *Burke* [2008] and *Burke et al.* [2009]. The ratio of the energies needed to raise the temperature by 100 K for summer and winter described in Figure 11 is 1.06, which means we have to add 6% more energy to the summer hemisphere in order to get the same temperature change, resulting in a smaller density change. In the summer hemisphere, the conductivity is larger and therefore the Joule heating is probably larger, allowing for more energy input and a larger temperature increase to result. On the other hand, in the winter hemisphere, the temperature starts out quite small, so that less energy input is needed to have a similar mass density reaction.

[25] Figure 12 shows the daily Joule heating in northern hemisphere averaged over 1999, 2000, and 2001 utilizing the assimilative mapping of ionospheric electrodynamics (AMIE) technique [*Richmond and Kamide*, 1988; *Richmond*, 1992; *Ridley and Kihn*, 2004]. The Joule heating is about twice in the summer than in the winter. So when both of these effects are taken into account (i. e, winter needing less energy for the same mass density change, and summer receiving more energy), the reaction in the mass density at 400 km between the summer and winter hemisphere may not be very different at all. During the equinoxes, though the background state is roughly the same. The southern hemisphere may react stronger to external driving due to the differences in magnetic field topology. It is uncertain why the vernal equinox would be favored in this explanation though.

6. Summary and Conclusions

[26] Thermospheric densities derived from the CHAMP/STAR accelerometer provide the chance to investigate the hemispheric asymmetry of the thermospheric response to geomagnetic storms with a global coverage at approximately 400 km altitude. In the present study, the thermospheric density response for the geomagnetic storm event of 03–07 April 2004 is first examined. Then a statistical analysis is conducted on 102 storm events from 01 May 2001 to 31 December 2007 under the conditions of *Dst* index < -50 and *Ap* index > 50. Analysis of the above storm events show some expected and some unexpected hemispheric differences. The observations and the conclusions are summarized below.

[27] First, for the storm event that occurred on 03–07 April 2004, the maximum density enhancement averaged across the dayside southern polar region is about 1.5∼2 times of that in the northern polar region under strong storm driving conditions (*Ap* index ≥ 30). Asymmetries are observed in the nighttime density response too, although with weaker hemispheric differences. This hemispheric asymmetry can also be observed when the linear dependences of the thermospheric density on the *Dst* and *Ap* indices are explored. The slope of the fitted line in the southern polar region is 50% greater than that in the northern polar region. The intercept of the fitted lines, which represent the densities under undisturbed conditions, is a little bit larger in northern polar region due to higher scale height induced by slightly warmer conditions in northern hemisphere, expected for the solar conditions. These results indicated that the southern hemisphere is more susceptible to strong driving conditions.

[28] Second, the seasonal variation of the intercepts and the slopes of the fitted lines between the thermospheric densities and *Dst* and *Ap* indices are depicted based on 102 storm events. For the fluctuation of intercepts, the summer hemisphere consistently has the larger density with the crossover occurring near the equinoxes. According to previous studies [e.g., *Emmert et al.*, 2008; *Qian et al.*, 2009], the baseline (i.e., the intercept) should be very dependent on season, with the hemisphere receiving the largest amount of sunlight having the largest density, which is what is observed. When the seasonal variability of the density is investigated on its own, the trend is similar to the intercept trend with the summer hemisphere having a larger density. The details in each hemisphere are different, though. The southern hemisphere shows a clear, symmetric variation from summer, where it peaks, to winter, where it minimizes. On the other hand, in the northern hemisphere, the densities show little variability with season, although there is a small peak near either the spring equinox (in the density variations) or autumnal equinox (in the intercepts). There is no clear explanation for what causes this hemispheric difference in behavior.

[29] Third, for the variation of the slopes, it was expected that the southern hemisphere would have a larger reaction the majority of the time, due to the asymmetry in the magnetic field topology. What was found, though, is that the hemispheres react about the same in all seasons except vernal equinox. It is suggested that during summer and winter,

competing effects cancel each other; i.e., the summer hemisphere probably receives more energy resulting in a larger temperature change, but the winter hemisphere needing a smaller temperature change to result in a similar mass density change. It is uncertain why the vernal and autumnal equinoxes differ, though.

[30] **Acknowledgments.** The authors acknowledge the GeoForschungsZentrum Potsdam, Germany (http://www.gfz-potsdam.de). The authors also thank E. K. Sutton (http://sisko.colorado.edu/sutton/data.html), who provided data of the CHAMP satellite used for this study. This work was supported by NSF grants ANT 0838828 and ANT 0838861, NASA grant NNG04GK18G, the National Natural Science Foundation of China (41174134 and 40904036), and the National Important basic Research Project of China (2011CB811405). The solar wind Interplanetary magnetic field data used for this study were downloaded from the Web site of ACE spacecraft: http://www.srl.caltech.edu/ACE/ASC. The *Ap* and *Dst* indices data were acquired from Coordinate Data Analysis Web: http://cdaweb.gsfc.nasa.gov/. The storm sudden commencements data were provided by ftp://ngdc.noaa.gov/STP/SOLAR_DATA. The DMSP satellite data was obtained from http://cindispace.utdallas.edu/DMSP/.

[31] Robert Lysak thanks the reviewers for their assistance in evaluating this paper.

References

Bruinsma, S., D. Tamagnan, and R. Biancale (2004), Atmospheric densities derived from CHAMP/STAR accelerometer observations, *Planet. Space Sci.*, *52*, 297–312, doi:10.1016/j.pss.2003.11.004.

Bruinsma, S., J. M. Forbes, R. S. Nerem, and X. Zhang (2006), Thermosphere density response to the 20–21 November 2003 solar and geomagnetic storm from CHAMP and GRACE accelerometer data, *J. Geophys. Res.*, *111*, A06303, doi:10.1029/2005JA011284.

Burke, W. J. (2008), Stormtime energy budgets of the global thermosphere, in *Mid-latitude Ionospheric Dynamics and Disturbances*, *Geophys. Monogr. Ser.*, vol. 181, edited by P. M. Kintner, pp. 235–246, AGU, Washington, D. C.

Burke, W. J., C. S. Lin, M. P. Hagan, C. Y. Huang, D. R. Weimer, J. O. Wise, L. C. Gentile, and F. A. Marcos (2009), Storm time global thermosphere: A driven-dissipative thermodynamic system, *J. Geophys. Res.*, *114*, A06306, doi:10.1029/2008JA013848.

Burns, A. G., T. L. Killeen, G. R. Carignan, and R. G. Roble (1995), Large enhancements in the O/N_2 ratio in the evening sector of the winter hemisphere during geomagnetic storms, *J. Geophys. Res.*, *100*, 14,661–14,672, doi:10.1029/94JA03235.

Christiansen, F., V. O. Papitashvili, and T. Neubert (2002), Seasonal variations of high-latitude field-aligned currents inferred from Ørsted and Magsat observations, *J. Geophys. Res.*, *107*(A2), 1029, doi:10.1029/2001JA900104.

Collin, H. L., W. K. Peterson, O. W. Lennartsson, and J. F. Drake (1998), The seasonal variation of auroral ion beams, *Geophys. Res. Lett.*, *25*, 4071–4074, doi:10.1029/1998GL900090.

Demars, H. G., and R. W. Schunk (2007), Thermospheric response to ion heating in the dayside cusp, *J. Atmos. Sol. Terr. Phys.*, *69*, 649–660, doi:10.1016/j.jastp.2006.11.002.

Emmert, J. T., J. M. Picone, and R. R. Meier (2008), Thermospheric global average density trends, 1967–2007, derived from orbits of 5000 near-Earth objects, *Geophys. Res. Lett.*, *35*, L05101, doi:10.1029/2007GL032809.

Erlandson, R. E., and L. J. Zanetti (1998), A statistical study of auroral electromagnetic ion cyclotron waves, *J. Geophys. Res.*, *103*, 4627–4636, doi:10.1029/97JA03169.

Forbes, J. M., R. Gonzalez, F. A. Marcos, D. Revelle, and H. Parish (1996), Magnetic storm response of lower thermosphere density, *J. Geophys. Res.*, *101*, 2313–2320, doi:10.1029/95JA02721.

Fuller-Rowell, T. J. (1998), The "thermospheric spoon": A mechanism for the semiannual density variation, *J. Geophys. Res.*, *103*, 3951–3956, doi:10.1029/97JA03335.

Fuller-Rowell, T. J., M. V. Codrescu, R. J. Moffett, and S. Quegan (1994), Response of the thermosphere and ionosphere to geomagnetic storms, *J. Geophys. Res.*, *99*, 3893–3914, doi:10.1029/93JA02015.

Griffis, M., J. S. Nisbet, and E. Bleuler (1981), Particle and Joule heating of the neutral polar thermosphere in cusp region using atmosphere Explorer-C satellite measurements, *Adv. Space Res.*, *1*, 27–30, doi:10.1016/0273-1177(81)90413-0.

Huang, C.-S., J. C. Foster, L. P. Goncharenko, P. J. Erickson, W. Rideout, and A. J. Coster (2005), A strong positive phase of ionospheric storms observed by the Millstone Hill incoherent scatter radar and global GPS network, *J. Geophys. Res.*, *110*, A06303, doi:10.1029/2004JA010865.

Jacchia, L. G. (1977), Thermospheric temperature, density, and composition: New models, *SAO Spec. Rep. 375*, Smithson. Inst., Washington, D. C.

Johnson, F. S., and B. Gottlieb (1970), Eddy mixing and circulation at ionospheric levels, *Planet. Space Sci.*, *18*, 1707–1718, doi:10.1016/0032-0633(70)90004-8.

Koustov, A. V., G. Y. Khachikjan, R. A. Makarevich, and C. Bryant (2009), On the SuperDARN cross polar cap potential saturation effect, *Ann. Geophys*, *27*, 3755–3764, doi:10.5194/angeo-27-3755-2009.

Kumamoto, A., and H. Oya (1998), Asymmetry of occurrence-frequency and intensity of AKR between summer polar region and winter polar region sources, *Geophys. Res. Lett.*, *25*, 2369–2372, doi:10.1029/98GL01715.

Liu, H., and H. Lühr (2005), Strong disturbance of the upper thermospheric density due to magnetic storms: CHAMP observations, *J. Geophys. Res.*, *110*, A09S29, doi:10.1029/2004JA010908.

Liu, H., H. Lühr, V. Henize, and W. Köhler (2005), Global distribution of the thermospheric total mass density derived from CHAMP, *J. Geophys. Res.*, *110*, A04301, doi:10.1029/2004JA010741.

Lühr, H., M. Rother, W. Köhler, P. Ritter, and L. Grunwaldt (2004), Thermospheric up-welling in the cusp region: Evidence from CHAMP observations, *Geophys. Res. Lett.*, *31*, L06805, doi:10.1029/2003GL019314.

Lukianova, R., and F. Christiansen (2008), Modeling the UT effect in global distribution of ionospheric electric fields, *J. Atmos. Sol. Terr. Phys.*, *70*, 637–645, doi:10.1016/j.jastp.2007.08.047.

Lukianova, R., C. Hanuise, and F. Christiansen (2008), Asymmetric distribution of the ionospheric electric potential in the opposite hemispheres as inferred from the SuperDARN observations and FAC-based convection model, *J. Atmos. Sol. Terr. Phys.*, *70*, 2324–2335, doi:10.1016/j.jastp.2008.05.015.

Mayr, H. G., I. Harris, and N. W. Spencer (1978), Some properties of upper atmosphere dynamics, *Rev. Geophys.*, *16*, 539–565.

Meier, R. R., G. Crowley, D. J. Strickland, A. B. Christensen, L. J. Paxton, D. Morrison, and C. L. Hackert (2005), First look at the 20 November 2003 superstorm with TIMED/GUVI: Comparisons with a thermospheric global circulation model, *J. Geophys. Res.*, *110*, A09S41, doi:10.1029/2004JA010990.

Neubert, T., and F. Christiansen (2003), Small-scale, field-aligned currents at the top-side ionosphere, *Geophys. Res. Lett.*, *30*(19), 2010, doi:10.1029/2003GL017808.

Newell, P. T., C.-I. Meng, and K. M. Lyons (1996), Suppression of discrete aurorae by sunlight, *Nature*, *381*, 766–767, doi:10.1038/381766a0.

Paetzold, H. K., and H. Zschörner (1961), An annual and a semiannual variation of the upper air density, *Geofis. Pura Appl.*, *48*, 85–92, doi:10.1007/BF01992371.

Pettigrew, E. D., S. G. Shepherd, and J. M. Ruohoniemi (2010), Climatological patterns of high-latitude convection in the Northern and Southern Hemispheres: Dipole tilt dependencies and interhemispheric comparisons, *J. Geophys. Res.*, *115*, A07305, doi:10.1029/2009JA014956.

Prölss, G. W. (1980), Magnetic storm associated perturbations of the upper atmosphere: Recent results obtained by satellite-borne gas analyzers, *Rev. Geophys.*, *18*, 183–202.

Prölss, G. W. (1987), Storm-induced changes in the thermospheric composition at middle latitudes, *Planet. Space Sci.*, *35*, 807–811, doi:10.1016/0032-0633(87)90041-9.

Qian, L., S. C. Solomon, and T. J. Kane (2009), Seasonal variation of thermospheric density and composition, *J. Geophys. Res.*, *114*, A01312, doi:10.1029/2008JA013643.

Reigber, C., H. Lühr, and P. Schwintzer (2002), CHAMP mission status, *Adv. Space Res.*, *30*, 129–134, doi:10.1016/S0273-1177(02)00276-4.

Richmond, A. D. (1992), Assimilative mapping of ionospheric electrodynamics, *Adv. Space Res.*, *12*, 59–68, doi:10.1016/0273-1177(92)90040-5.

Richmond, A. D., and Y. Kamide (1988), Mapping electrodynamic features of the high-latitude ionosphere from localized observations: Technique, *J. Geophys. Res.*, *93*, 5741–5759, doi:10.1029/JA093iA06p05741.

Ridley, A. J. (2007), Effects of seasonal changes in the ionospheric conductances on magnetospheric field-aligned currents, *Geophys. Res. Lett.*, *34*, L05101, doi:10.1029/2006GL028444.

Ridley, A. J., and E. A. Kihn (2004), Polar cap index comparisons with AMIE cross polar cap potential, electric field, and polar cap area, *Geophys. Res. Lett.*, *31*, L07801, doi:10.1029/2003GL019113.

Ridley, A. J., T. I. Gombosi, and D. L. DeZeeuw (2004), Ionospheric control of the magnetosphere: Conductance, *Ann. Geophys.*, *22*(2), 567–584, doi:10.5194/angeo-22-567-2004.

Rishbeth, H., T. J. Fuller-Rowell, and D. Rees (1987), Diffusive equilibrium and vertical motion in the thermosphere during a severe magnetic storm: A computational study, *Planet. Space Sci.*, *35*, 1157–1165, doi:10.1016/0032-0633(87)90022-5.

Shepherd, S. G., R. A. Greenwald, and J. M. Ruohoniemi (2002), Cross polar cap potentials measured with Super Dual Auroral Radar Network during quasi-steady solar wind and interplanetary magnetic field conditions, *J. Geophys. Res.*, *107*(A7), 1094, doi:10.1029/2001JA000152.

Shepherd, S. G., J. M. Ruohoniemi, and R. A. Greenwald (2003), Direct measurements of the ionospheric convection variability near the cusp/throat, *Geophys. Res. Lett.*, *30*(21), 2109, doi:10.1029/2003GL017668.

Sutton, E. K., J. M. Forbes, and R. S. Nerem (2005), Global thermospheric neutral density and wind response to the severe 2003 geomagnetic storms from CHAMP accelerometer data, *J. Geophys. Res.*, *110*, A09S40, doi:10.1029/2004JA010985.

Wang, H., H. Lühr, and S. Y. Ma (2005), Solar zenith angle and merging electric field control of field-aligned currents: A statistical study of the Southern Hemisphere, *J. Geophys. Res.*, *110*, A03306, doi:10.1029/2004JA010530.

Weimer, D. R. (1996), A flexible, IMF dependent model of high-latitude electric potentials having "space weather" applications, *Geophys. Res. Lett.*, *23*, 2549–2552, doi:10.1029/96GL02255.

Wilson, G. R., D. R. Weimer, J. O. Wise, and F. A. Marcos (2006), Response of the thermosphere to Joule heating and particle precipitation, *J. Geophys. Res.*, *111*, A10314, doi:10.1029/2005JA011274.